

(Tremmel & Taulbee, 2008). The flow field in the fan showed several characteristic features. With the averaging process, the blades disappear in the simulation but additional equation terms arise as the immersed boundary method (IBM), which represents the blade forces on the fluid. This method can save a lot of CPU time. These savings in computational cost make the CFD analysis of fans more economic.

Rafael showed simulation results of the unsteady flow of inlet, impeller and outlet flow in a squirrel cage fan, and summarized the characteristics of the three regions under different working conditions (Rafael, 2009). In addition, there are researchers using some mathematical methods to optimize fan. Kim used the response surface method to optimize the shape of a forward-curved-blade centrifugal fan (Kim and Seo, 2004).

Suárez find that there is a clear flow separation pattern in the blade to blade passages for all the operating conditions (Suarez *et al.* 2006). The discontinuous volute profile is widely used in the squirrel cage fan to meet the space limitation in the air conditioning system. However, it usually causes an obvious performance drop due to the unreasonable impeller-volute interaction. Wen used two design methods to enhance the aerodynamic performance of the fan installed in a limited space (Wen *et al.* 2016). They suggested that the design method of the downsized volute profile is more suitable for slight space limitation, while the design method of the partial flow volute profile is more suitable for significant space limitation. Wen indicates that an optimal elliptical inlet nozzle can reduce flow loss before fluid entering into the impeller passages and induce a tip flow pattern, contributing to promote the volume flow rate and suppress the leaking flow loss (Wen *et al.* 2013).

In addition to the experimental measurements, CFD and computational aeroacoustic (CAA) simulations were carried out to investigate the effects of different modifications on noise and performance of the fan (Darvish *et al.* 2015). It was shown that the tonal noise of the fan can effectively be reduced by making some geometrical modifications. Kind described a method for predicting flow behavior and performance for a squirrel cage fan (Kind, 1997). The fan is subdivided into three zones (inlet, blade, and volute). They believed that the goal of optimization should be focused on the blades.

For the blade part, the single arc and strong forward bending acceleration flow channel design method are widely adopted based on the current status of processing technology and cost. In such, the blade inlet angle of many squirrel cage fans is about 80 degrees and the blade inlet angle is about 10 degrees. The total pressure efficiency of most squirrel cage fans can only reach to 45% (Rafael, 2009; Kim and Seo, 2004; Suarez *et al.* 2006; Wen *et al.* 2016; Wen *et al.* 2013). A larger inlet angle not only causes a large airflow impact at the blade inlet, but also makes the airflow difficult to enter the blade passages.

Although there are many studies about the numerical simulation works and optimization works of squirrel cage fans. However, there are little studies on blade optimization, especially for small size squirrel cage fans in fan coil of air conditions. Therefore, it is imperative to do some studies on blade optimization of squirrel cage fans.

In this paper, the single arc blade is replaced by double-arc blade in order to optimize the blade model and improve the static pressure and total pressure efficiencies of the fan. For the numerical analysis, results validate the positive effects of the double arc blade design method of squirrel cage fan on the aerodynamic performance.

2. DESIGN METHOD

2.1 Design Method for Double arc Blade

The squirrel cage fan is provided by Yilida Ventilator Co., Ltd. and the model is SYP130-190. Figures 1 show the configuration of the squirrel cage fan SYP130-190. Figure 1(a) shows the axial sketch and Fig. 1(b) shows the radial sketch of the fan. The unit of the dimension given in Fig. 1 is millimeter. Figure 1(c) shows the configuration of the squirrel cage fan which includes the impeller and the volute. It can be seen that the fan is symmetrical. Although the simulation is carried out for the whole fan, the numerical simulation results in impeller will be provided only for half of the fan.

The geometrical parameters of the impeller are shown in Table 1. In addition to the inlet angle, outlet angle, blade arc length and blade radius of curvature, other parameters in the table are constant during the optimization process.

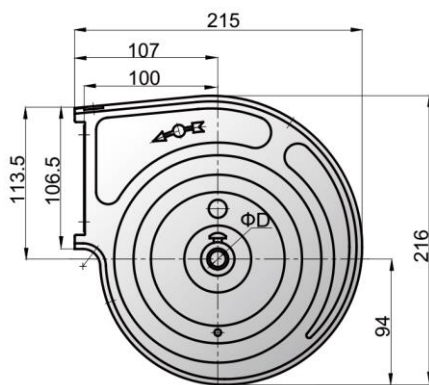
Table 1 Geometrical parameters of the impeller

Parameter	Size
$D1$ (mm)	105
$D2$ (mm)	133
$\beta 1$ (deg.)	79.0
$\beta 2$ (deg.)	9.3
Z	38
d (mm)	189
R (mm)	9

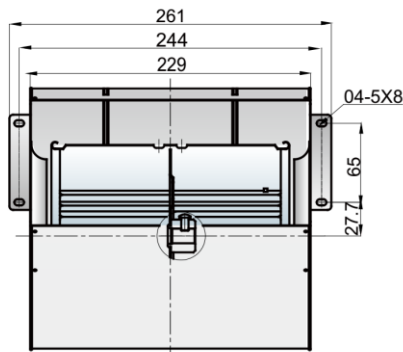
Figure 2 shows sketch of a single circular-arc blade in the impeller. The single-arc blade extends from point A_0 to B_0 and the blade model is determined by the inlet angle $\beta 1_0$ and the outlet angle $\beta 2_0$. As shown in Fig. 2(b), O_0 is the arc center of the single arc blade and R_0 is the radius of the single arc blade, where α_0 is the angle of the single arc.

The single arc blade model can be shaped by only two parameters of inlet and outlet angle of blade when the inner and outer diameters of the impeller are constant. However, it is easy to cause flow blockage near the inlet of blades by adjusting the shape of blades based on these two parameters. The size of the inlet angle of blade is affected by some factors. For example, accelerated blade design method mostly used to squirrel cage fan, which

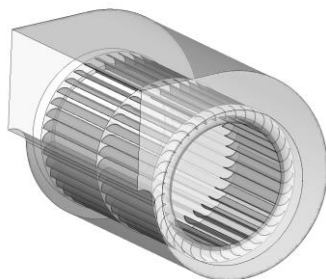
requires the blade inlet angle to be as large as possible. It can be seen that the range of the inlet angle of blade is restricted. The airflow may impact directly the inlet part of blade caused by the large angle of inlet blade. This phenomenon may leads to flow separation at the inlet part of the blade. It is difficult to meet the design principle for the accelerating blade channel with a small inlet angle. In addition, small inlet angle means long length of the blade, which may cause much more energy loss. However, the blade is formed by an arc with a smaller radius of curvature in the inlet section, then an arc section with a larger arc radius is used in the outlet section to form the outlet section. Because of the obvious arc structure of the inlet section, the airflow in the inlet section is prevented from directly hitting the blade.



(a) axial sketch

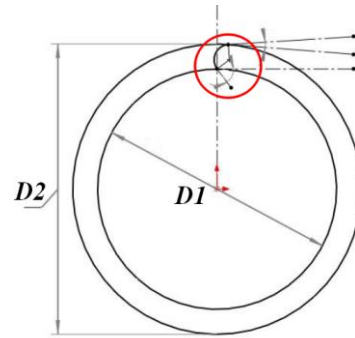


(b) radial sketch

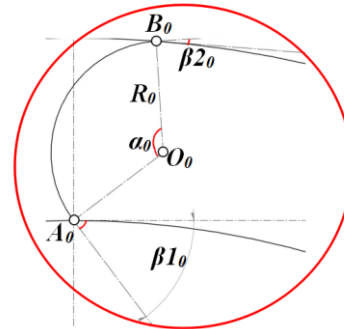


(c) configuration of the fan

Fig. 1. Configuration of SYP130-190.



(a) single arc blade in impeller



(b) single arc blade

Fig. 2. Sketch of single arc blade.

Therefore, the design method of double arc blade is introduced with four parameters: the inlet angle and the outlet angle, the first circle radius of curvature and the first circle center angle. The orthogonal optimization method is used to get the best blade model in the case of multiple parameters and levels. The double circular arc blade is comprised of two arcs, so the inlet angle of the blade is actually the inlet angle of the first circular blade, and the outlet angle of the blade is the outlet angle of the second circular blade.

The single arc blade is replaced by double-arc blade in order to optimize the blade model and improve the static pressure and total pressure efficiency of the fan. The inner or outer diameters and number of blades remain as constant, and the shape of the volute is not changed. Only the inlet and outlet angles of the blades are changed. At the same time, four parameters R_1 , α_1 , R_2 , α_2 are introduced to the optimization of the blade. Figure 3 shows the sketch of the double arc blade structure. O_1 is the center of first circular arc and O_2 is the center of second circular arc. A_1 is the starting point of the double arc blade and B_2 is the end point of the double arc blade. The double arc blade is got when 4 parameters of these 6 parameters β_{11} , β_{22} , α_1 , R_1 , α_2 , R_2 are determined.

The orthogonal experimental design method is used to optimize blade model base on the parameters β_{11} , β_{22} , R_1 , α_1 . According to the characteristic of the squirrel cage fan, the theoretical range of the inlet angle and the outlet angle is from 0 to 90 degrees. R_1 and α_1 are related to β_{11} .

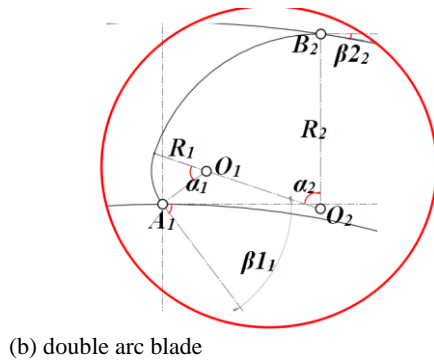
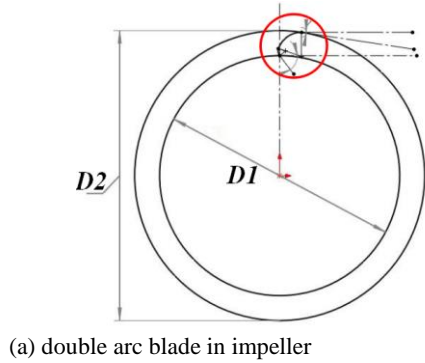


Fig. 3. Sketch of the double arc blade.

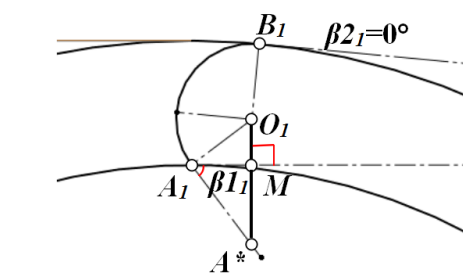
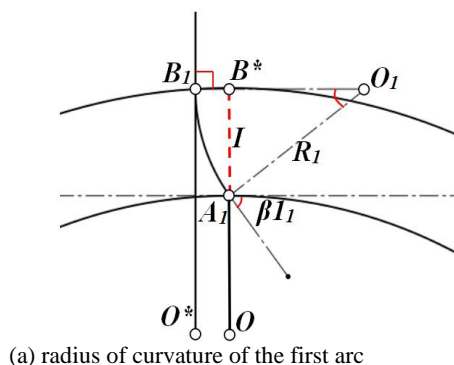


Fig. 4. Sketch of the first arc.

The theoretical range of R_1 and α_1 for blade is important. The maximum of the radius of curvature R_1 of the arc and the angle of the center α_1 are required. As shown in Fig. 4(a), point O is the center of the impeller, and B^* and O^* are auxiliary points, where B^* , A_1 , and O are collinear, B_1O^* is parallel to B^*A_1 , and B_1O_1 is perpendicular to B_1O^* , and arc B_1A_1 is tangent to line segment B_1O^* and point B_1 . It is easy to get the relationship $\sin(90^\circ - \beta_{11}) = I/R_1$, where $I \approx (D_2 - D_1)/4$. Therefore, the

maximum of R_1 (A_1O_1 shown in Fig. 4(a)) is $I/\sin(90^\circ - \beta_{11})$.

As shown in Fig. 4(b), the three points A^* , M , and O_1 are collinear. The line segment O_1A^* is perpendicular to the line segment A_1M intersected at point M . It is easy to get that the angle A_1O_1M equal to β_{11} . The arc B_1A_1 is tangent to the first arc exit arc and B_1 point, so that the first arc exit angle β_{21} is 0° and the central angle $A_1O_1B_1$ can be the maximum value. As shown in Fig. 4(b), the angle $A_1O_1B_1$ is the maximum central angle of the first arc. The size of angle $A^*O_1B_1$ can be approximated as 180° . Because of the angle $A_1O_1M = \beta_{11}$, the limit value of the first circle arc angle in Eq.(1) is $180^\circ - \beta_{11}$.

$$R_1 = R^* \cdot I / \sin(90^\circ - \beta_{11}) \quad (1)$$

$$\alpha_1 = \alpha^* \cdot (180^\circ - \beta_{11}) \quad (2)$$

The parameters chosen in the project should include all available values as much as possible. However, it is impossible to try every value of blade parameters. Therefore, proportional parameters help to get suitable range of parameters of the blade. The proportional parameter of R_1 is R^* and the proportional parameter of α_1 in Eq.(2) is α^* . When the proportional parameter is set, the radius of curvature and the central angle of the first arc is then determined by multiplying their maximum by proportional parameter, respectively.

2.2 Orthogonal Test

It is unreasonable to optimize the fan with a lot of experiments included all cases. The more parameters considered the more experiments are needed. It needs to use orthogonal experimental design to complete optimization with several parameters. In this paper, the optimization of the fan impeller blades is mainly optimized for the double arc blade profile. The four factors β_1 , β_2 , R^* , α^* are used to optimize the installation angle of each section of the blade. In order to obtain the optimal interval of 4 parameters, multiple orthogonal experiments were carried out, and the values of the four parameters were continuously adjusted to obtain a better result. In this paper, three orthogonal experiments were performed and there are 4 factors in each orthogonal experiment. There are 4 levels shown in Table 2 for each factor and 16 test groups in first orthogonal test and 5 levels shown in Table 3 for each factor and 25 test groups in second orthogonal test, 3 levels shown in Table 4 for each factor and the 9 test groups in third orthogonal test shown in Table 5.

Table 2 First orthogonal test

Level	Factor			
	β_{11}	β_{22}	α^*	R^*
1	26	9	0.425	0.5
2	39	18	0.5	0.595
3	52	27	0.575	0.69
4	65	36	0.65	0.785

Table 3 Second orthogonal test

Level	Factor			
	$\beta 1_1$	$\beta 2_2$	α^*	R^*
1	55	3	0.6	0.35
2	60	6	0.65	0.4
3	65	9	0.7	0.45
4	70	12	0.75	0.5
5	75	15	0.8	0.55

Table 4 Third orthogonal test

Level	Factor			
	$\beta 1_1$	$\beta 2_2$	α^*	R^*
1	53	1	0.73	0.38
2	55	3	0.75	0.4
3	57	5	0.77	0.42

Table 5 Orthogonal table of the third test

Test	Factor			
	$\beta 1_1$	$\beta 2_2$	α^*	R^*
1	53	1	0.73	0.38
2	53	3	0.75	0.4
3	53	5	0.77	0.42
4	55	1	0.75	0.42
5	55	3	0.77	0.38
6	55	5	0.73	0.4
7	57	1	0.77	0.4
8	57	3	0.73	0.42
9	57	5	0.75	0.38

The orthogonal test results are analyzed by visual analysis method after the orthogonal test for the double arc blade is designed. Then the optimal parameter combination of each test is got. The optimal numerical simulation results of the three tests are shown in Table 6.

Table 6 Optimal combinations of orthogonal tests (numerical simulation results)

Factor				Aerodynamic characteristics		
$\beta 1_1$	$\beta 2_2$	α^*	R^*	P_{st}	P_t	η
65	9	0.65	0.5	66.3	82.2	42.5
55	3	0.75	0.4	69.4	90.6	45.1
53	1	0.77	0.42	70.6	92.6	45.4
53	1	/	/	67.3	83.8	43.5

The optimal result obtained by the last orthogonal experiment is taken as the final optimization result. Then the optimal result is compared with result of the original model. One numerical simulation of

single arc blade fan is added to compare with the double arc blade fan. The inlet and outlet angles of the single arc are same as the optimal double arc blade fan. As shown in Table 6, the simulation performance of the double arc blades fan with the same inlet and outlet angles is better than the single arc blade fan.

3. RESULTS AND DISCUSSIONS

The computational fluid dynamics method is based on the basic governing equations of fluid mechanics: continuous equations, momentum equations and energy equations. The laws of physics on which these three equations are based are mass conservation, Newton's second law, and energy conservation. The internal flow of a squirrel cage fan can be considered as an incompressible fluid flow, while the numerical simulations herein do not involve heat transfer. In this paper, ANSYS is used to numerically calculate the three-dimensional flow field and the standard k-epsilon turbulence model is adopted.

$$\frac{\partial \rho}{\partial t} + \frac{\partial}{\partial x_i}(\rho u_i) = 0 \tag{3}$$

$$\frac{\partial \rho u_i}{\partial t} + \frac{\partial}{\partial x_j}(\rho u_i u_j) = -\frac{\partial P^*}{\partial x_i} + \tag{4}$$

$$\frac{\partial}{\partial x_j} \left[\mu_e \left(\frac{\partial u_i}{\partial x_j} + \frac{\partial u_j}{\partial x_i} \right) \right] + S_i$$

Where ρ is the fluid density, P^* is the translation pressure (including turbulent energy and centrifugal force), S is the sum of the volume force source terms, i, j is the free subscript, and μ_e is the effective viscosity coefficient, where $\mu_e = \mu + \mu_t$, μ is the molecular viscosity coefficient, and μ_t is the turbulent eddy viscosity coefficient.

In order to close the solution equation, two k and ϵ quantities and their related equations are added.

$$\frac{\partial(\rho k)}{\partial t} + \frac{\partial}{\partial x_i}(\rho u_i k) = \frac{\partial}{\partial x_i} \left[\left(\mu + \frac{\mu_t}{\sigma_k} \right) \frac{\partial k}{\partial x_i} \right] \tag{5}$$

$$+ P_k - \rho \epsilon + P_{kb}$$

$$\frac{\partial(\rho \epsilon)}{\partial t} + \frac{\partial}{\partial x_i}(\rho u_i \epsilon) = \frac{\partial}{\partial x_i} \left[\left(\mu + \frac{\mu_t}{\sigma_\epsilon} \right) \frac{\partial \epsilon}{\partial x_i} \right] \tag{6}$$

$$+ \frac{\epsilon}{k} (C_{\epsilon 1} P_k - C_{\epsilon 2} \rho \epsilon + C_{\epsilon 1} P_{eb})$$

The constant term $C_{\epsilon 1}=1.44$, $C_{\epsilon 2}=1.92$, $\sigma_k=1.0$, $\sigma_\epsilon=1.3$, P_{ek} , P_{eb} represents the energy term generated by buoyancy, and P_k represents the energy term generated by the viscous force.

Since the model fan is a dual air inlet and a single air outlet fan, the inlet boundary conditions are pressure boundary conditions and the outlets are flow boundary conditions. A pair of moving and static surfaces are used for data transfer between the

rotating parts and the non-rotating parts in the squirrel cage fan. The blades of the model fan and the wall following the rotation of the impeller are set as rotational boundaries, and the other walls are stationary walls. The non-slip boundary condition is used at the solid wall and the near wall is treated with a standard wall function. The spatial discretization of the convection term adopts the second-order upwind style, the spatial discretization of the diffusion term adopts the central difference scheme with second-order precision, and the coupling of velocity and pressure is realized by SIMPLE algorithm.

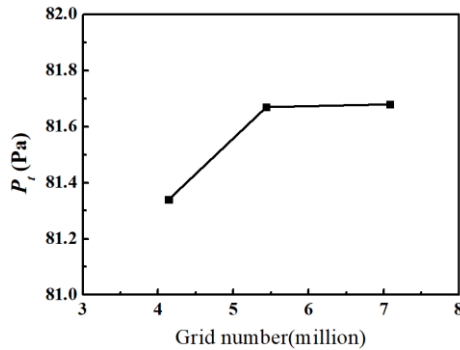


Fig. 5. Grid number with P_t .

The commercial software Fluent is used to simulate the squirrel cage fan SYP-130-190. The grid-independence verification results are shown in Fig. 5. The number of mesh is 4.14 million, 5.44 million, and 7.08 million respectively. As shown in Fig. 5, the ordinate is the simulated total pressure of the fan. When the number of mesh is more than 4.14 million, the difference in the total pressure of the fans under different grid numbers is less than 1%. Therefore, this paper uses the 5.44 million grids in the numerical calculation of the stationary flow. This number of grids has a good calculation cost and can predict the flow characteristics of the fan well.

The experimental installation is shown in Fig. 6. In the air outlet type experiment of the centrifugal fan, the flow rate is measured by using multiple nozzles. In the measurement of flow, the flow should actually have no eddy currents. Four pressure measuring holes are uniformly arranged in the cross section of the circular air chamber before and after the nozzle, and the pressure measuring hole is 38 ± 6 mm from the nozzle wall surface, and the average value of the four pressure measuring holes is taken as the pressure measurement value. The flow rate Q_m of the centrifugal fan is calculated from the pressure difference ΔP measured before and after the nozzle.

$$Q_m = \varepsilon \sum_1^n \left(a_i d_i^2 \right) \frac{\pi}{4} \sqrt{2\rho\Delta P} \quad (7)$$

In the formula, the square of the diameter of each open nozzle is multiplied by the sum of their respective flow coefficients.

In this experiment, the installation method of the

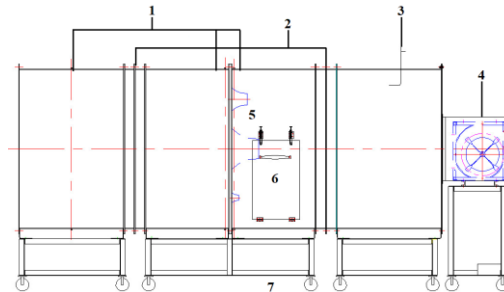
forward squirrel cage centrifugal fan is freely imported, that is, the inlet of the squirrel cage fan is considered to be atmospheric, and the inlet full pressure and the inlet static pressure of the squirrel cage fan are both atmospheric pressure. Four pressure measuring holes are evenly arranged at the middle section of the wind chamber inlet and the rectifying net, and the average value of the four pressure measuring holes is the static pressure value at the exit of the squirrel cage fan. The difference between the static pressure values of the inlet and outlet of the squirrel cage fan is the static pressure of the squirrel cage fan. From the mass flow of the squirrel cage ventilator and the cross-sectional area at the outlet, the airflow velocity at the exit of the squirrel cage ventilator and, ie, the dynamic pressure of the squirrel cage ventilator, can be calculated. The sum of the static pressure and the dynamic pressure at the exit of the squirrel cage fan is the full pressure at the exit of the squirrel cage fan. The full pressure difference at the inlet and outlet of the squirrel cage fan is the full pressure of the squirrel cage fan.

$$P_t = P_{st} + P_d \quad (8)$$

The formula for calculating the total pressure efficiency η of the centrifugal fan is as follows

$$\eta = \frac{N_e}{N} = \frac{P_t \cdot Q_m}{1000N} \quad (9)$$

In addition to mesh-independence verification, the simulation results of the original model are compared with the experimental results.



(a) sketch of the experimental system—1, pressure taps; 2, flow-regulating honeycomb; 3, temperature and humidity gauge; 4, auxiliary fan; 5, multiple nozzles; 6, entrance of air duct



(b) photograph of the test facility
Fig. 6. Experimental facility.

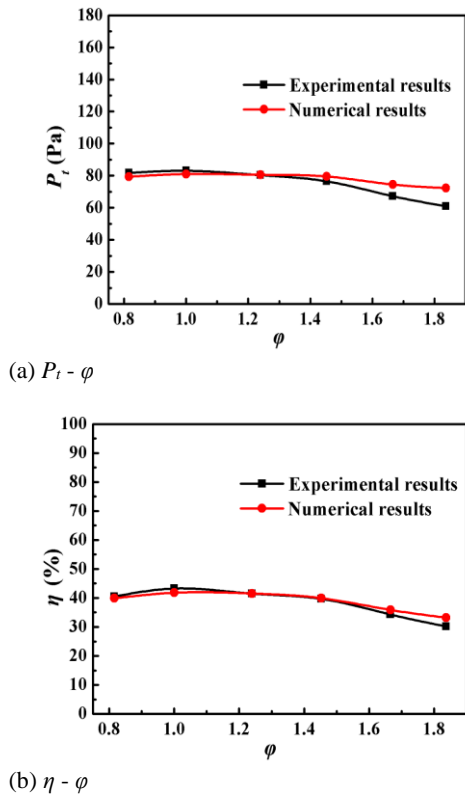


Fig. 7. Comparison of aerodynamic characteristic with experiment and numerical results.

Figure 7 shows the total pressure (a) and efficiency (b) with rate flow of SYP130-190 respectively. The abscissas are non-dimensionalized flow rate $\varphi=Q/Q_n$, $\varphi=1$ indicates the flow rate at the highest efficiency point of operation. The numerical results do not match the experimental results well under the large massflow conditions. The blade with small thickness deformation occurs at the larger massflow condition. However, the numerical analysis does not take this deformation into account. But the difference between the numerical and experimental results is less than 4%.

As shown in Fig. 8, the total pressure and efficiency of the optimized model are increased compared with the original model. The total pressure of the optimized model is increased by 11.3 Pa at $\varphi=1.24$, meanwhile the total pressure efficiency is increased by 4.7%. The total pressure of the optimized model is increased by 11.7Pa at $\varphi=1$, meanwhile the total pressure efficiency is increased by 3.7%. It proves that the performance of the fan can be improved by the double arc blade design method.

As shown in Fig. 9, the static pressure of the optimized model is higher than that of the original model at all operating points. The static pressure increases by 6.1Pa at $\varphi=1$, and static pressure increases by 11.6Pa at $\varphi=1.45$. In the two operating conditions with larger flow, the static pressure increased slightly. Since the orthogonal optimization target of this paper is the static pressure of the fan, the static pressure of all the operating points of the improved model as shown in the figure is improved compared with the original

model. This also shows that the purpose of optimization in this paper has been achieved.

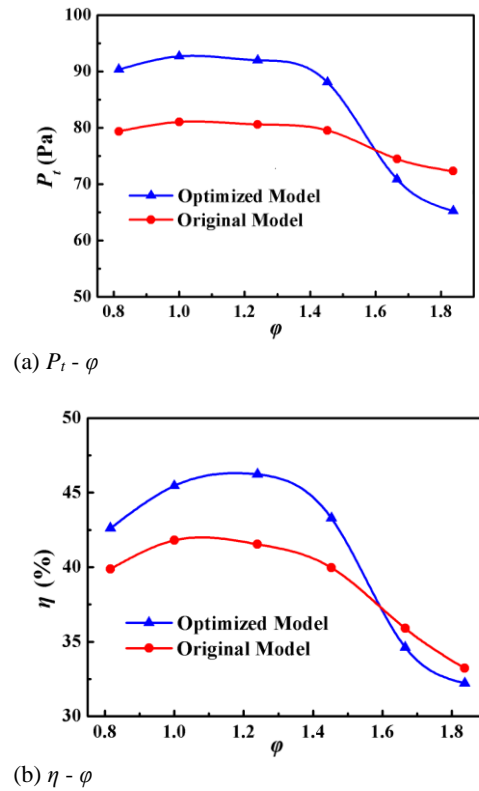


Fig. 8. Comparison of aerodynamic characteristics with original model and optimized model.

All the contours, streamline diagrams, and line graphs in the following paragraphs of the optimized model are compared with the original model under the rated conditions $\varphi=1$ with the same rotate speed.

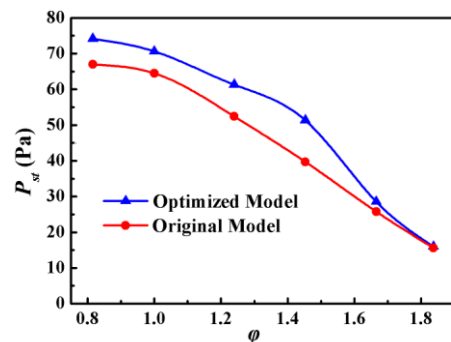
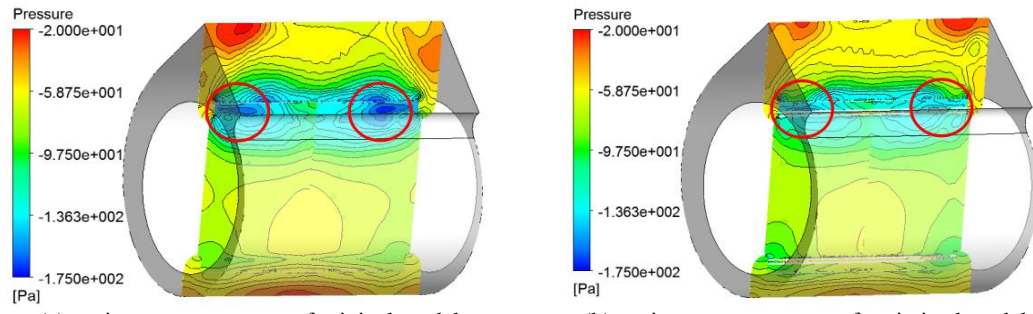
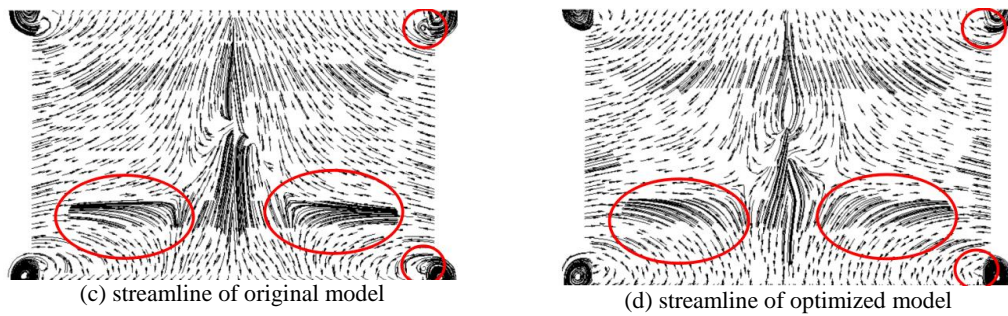
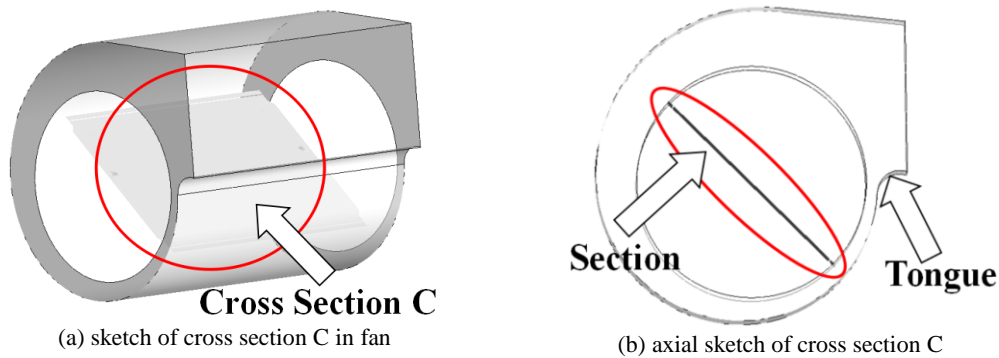


Fig. 9. Comparison of static pressure with original model and optimized model of SYP130-190.

Figure 10 shows the cross section B in the fan. In the section of this position, the exit of the original model blade is close to the side wall surface of the volute, and there is a clear low-pressure zone. In the same position in the optimization model, the static pressure distribution is more uniform and there is no obvious low pressure region. The non-uniform pressure region inside the fan easily causes vortex and energy loss. The non-uniform pressure



(a) static pressure contour of original model (b) static pressure contour of optimized model
Fig. 10. Comparison of the contour of cross section B in fan with original model and optimized model.



(c) streamline of original model (d) streamline of optimized model
Fig. 11. Comparison of streamline of cross section C with original model and optimized model.

distribution in the fan will increase the friction effect and energy loss in the gas transport process. Therefore, the low pressure region (the red circle) in Fig. 10 is eliminated in optimized model, and the pressure is also more uniform along the radial direction of the impeller in optimized model.

Figure 11 (a) and (b) show the cross section C in the fan. From Fig. 11 (c) and (d) (the same density of streamlines), it can be seen that the air flow is blocked on the bottom of cross section c in original model, and the streamline at the same position of improved model is more smooth. There are vortices near the volute side in original model, but there is no obvious vortex at the same position of improved model.

Kind and Tobin used a probe to measure a squirrel cage fan. They pointed out that the internal flow of the fan is very complicated (Kind and Tobin, 1990). Even at the point of maximum efficiency, there is a back flow can still be observed inside the flow path

of the blade. There are large vortexes at the inlet of the blade according to the literature (Tremmel and Taulbee, 2008; Suarez *et al.* 2006; Wen *et al.* 2016; Kind and Tobin, 1990; Fernandez *et al.* 2013). The numerical simulation of this paper also captures this phenomenon. The radial section of the impeller is taken to observe the flow in the blade. The section is located at the center of the left impeller and shown in Fig. 12. In order to show the specific position of the midpoint of the lines in cross section D, the lines are expanded with angle. Figure 12(b) shown the location of $\theta=0^\circ$ and $\theta=90^\circ$, and the region $\theta=20^\circ\sim 50^\circ$ is near the tongue.

As shown in Fig. 13, the vortex at the blade inlet is obvious in both original model and optimized model, but the vortexes are smaller in the optimized model. The quantitative analysis method was used to extract the relative velocity and static pressure distribution on the inlet and the outlet blade, and the difference between the original model and the optimization model was compared.

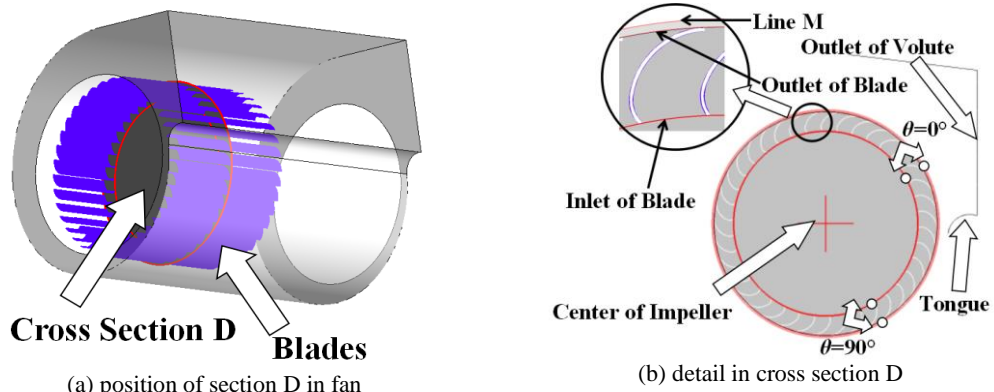


Fig. 12. Sketch of cross section D in fan.

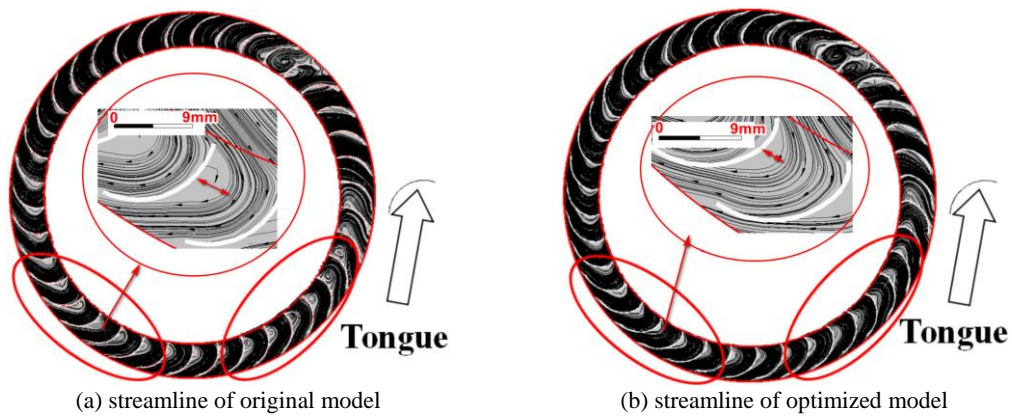


Fig. 13. Comparison of streamline of cross section D with original model and optimized model.

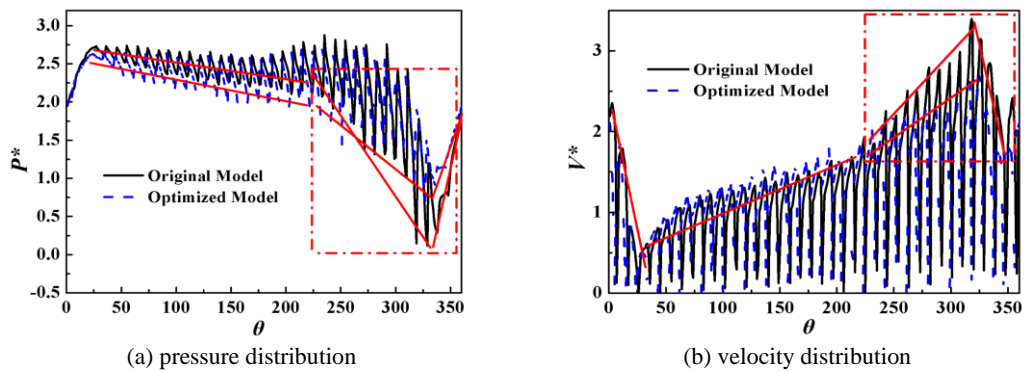


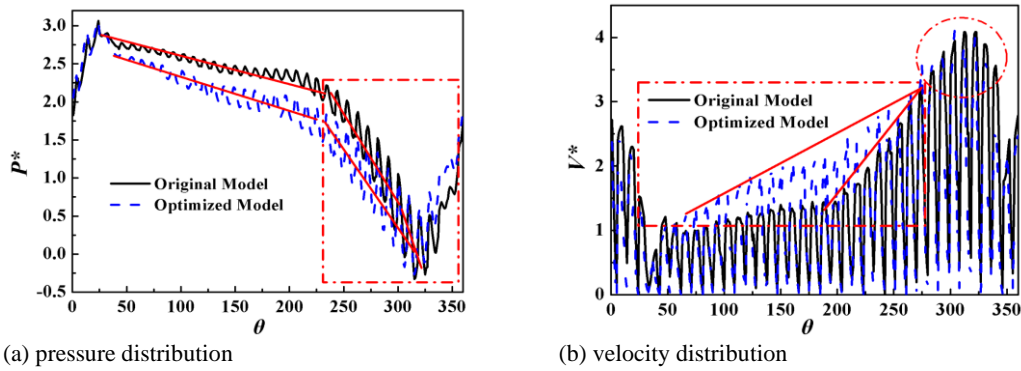
Fig. 14. Comparison of pressure and velocity distribution of blade inlet (in cross section D) with original model and optimized model.

The loop line positions of the blade inlet, blade outlet, and the extending of blade outlet (line M, extend the distance of 1mm from blade outlet) are shown in Fig. 12. P_l is the minimum static pressure on the blade surface, and its absolute value is 101089Pa. V_n is the average volute outlet velocity at the rated flow of the original model. The size of volute outlet is 229mm*106.5mm. As shown in the Fig. 14, the average velocity between the two models is not much different. However, the velocity distribution of the optimized model is more uniform in the region of $\theta=225^\circ\sim 325^\circ$.

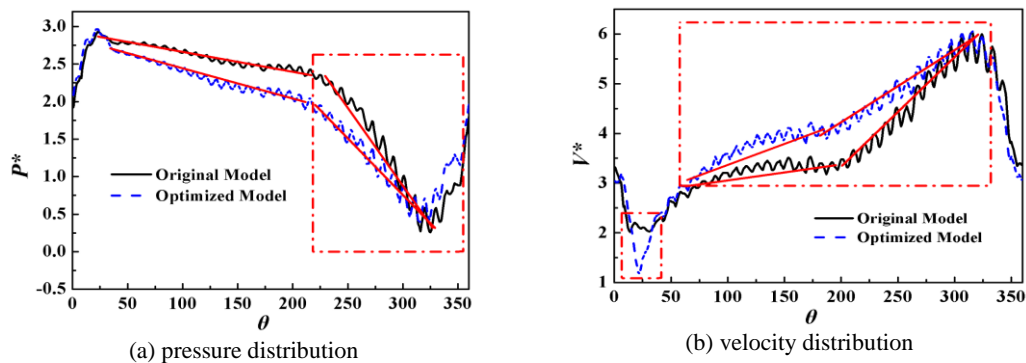
The velocity in the region near the outlet of the

spiral case in the original model is larger than that the velocity in the optimized model. The velocity difference results in the friction and energy loss between the air flows. The velocity distribution of the optimized model is more uniform and the static pressure is larger.

As shown in the Fig. 15, the maximum and minimum values of outlet pressure and velocity are almost the same, but their distributions are different. The velocity distribution of the optimized model is more uniform in the region of $\theta=50^\circ\sim 275^\circ$. The velocity in the region of $\theta=200^\circ\sim 300^\circ$ of the original model increases more heavily that may



(a) pressure distribution (b) velocity distribution
Fig. 15. Comparison of pressure and velocity distribution of blade outlet (in cross section D) with original model and optimized model.



(a) pressure distribution (b) velocity distribution
Fig. 16. Comparison of pressure and velocity distribution on circle line M (in cross section D) with original model and optimized model.

produce nonuniform velocity distribution. The circumferential velocity exhausted from the outlet of the original model forms jet-wake pattern which leads to strong shear flow, and results in more energy loss.

As shown in the Fig. 16, it is similar to the pressure distribution at the outlet of the blade. The pressure of the original model decreases rapidly in the region of $\theta=225^\circ\sim 325^\circ$, but the pressure of the optimized model decreases more flatly. In the region of $\theta=50^\circ\sim 325^\circ$, the velocity distribution of the optimization model is more uniform with less energy loss and better aerodynamic performance. It can also be seen that the velocity of $\theta=200^\circ\sim 300^\circ$ increases greatly in the original model, which indicates that the unreasonable design of the blade model will affect the velocity distribution in the volute.

4. CONCLUSIONS

In this paper, the single arc blade is replaced by double arc blade in order to obtain the blade model and improve the static pressure and total pressure efficiency of the fan.

The total pressure and efficiency of the optimized model are increased compared with the original model. The total pressure of the optimized model is increased by 11.3 Pa at $\varphi=1.24$, meanwhile the total pressure efficiency is increased by 4.7%. The total pressure of the optimized model is increased by

11.7Pa at $\varphi=1$, meanwhile the total pressure efficiency is increased by 3.7%. The static pressure is increased by 6.1Pa at $\varphi=1$, and static pressure increases by 11.6Pa at $\varphi=1.45$. Therefore, the design with double arc blade is able to improve the internal flow, and to enhance the aerodynamic performance of squirrel cage fans.

ACKNOWLEDGEMENTS

This work is supported by National Natural Science Foundation of China (51536008, 51579224), Zhejiang Province Science and Technology Plan Project (2017C34007), and Zhejiang Province Key Research and Development Plan Project (2018C03046).

REFERENCES

- Darvish, M., S. Frank, and O. Paschereit (2015). Numerical and Experimental Study on the Tonal Noise Generation of a Radial Fan, *Journal of Turbomachinery* 137(10), 1-9.
- Fernandez, O, P. García, and J. González (2013). Numerical Methodology for the Assessment of Relative and Absolute Deterministic Flow Structures in the Analysis of Impeller-Tongue Interactions for Centrifugal Fans, *Computers & Fluids* 86(7), 310-325.
- Kim, Y. and J. Seo (2004). Shape Optimization of

- Forward-Curved-Blade Centrifugal Fan with Navier-Stokes Analysis, *Journal of Fluids Engineering* 126(5), 735-742.
- Kind, J. (1997). Prediction of Flow Behavior and Performance of Squirrel-Cage Centrifugal Fans Operating at Medium and High Flow Rates, *Journal of Fluids Engineering* 119(3), 639-646.
- Kind, J. and G. Tobin (1990). Flow in a Centrifugal Fan of the Squirrel-Cage Type, *Journal of Turbomachinery* 112(1), 84-90.
- Rafael, T., C. Francisco, and S. Sandra (2009). Numerical Model for the Unsteady Flow Features of a Squirrel Cage Fan, *American Society of Mechanical Engineers*, 173-183.
- Suárez, V., B. Tajadura, and G. Pérez (2006). Numerical Simulation of the Unsteady Flow Patterns in a Small Squirrel-Cage Fan, *American Society of Mechanical Engineers*, 297-304.
- Tremmel, M. and D. Taulbee (2008). Calculation of the Time-Averaged Flow in Squirrel-Cage Blowers by Substituting Blades With Equivalent Forces, *Journal of Turbomachinery* 130(3), 538-544.
- Wen, X., D. Qi, and Y. Mao (2013). Experimental and Numerical Study on the Inlet Nozzle of a Small Squirrel-Cage Fan, *Proceedings of the Institution of Mechanical Engineers, Part A: Journal of Power and Energy* 227(4), 450-463.
- Wen, X., Y. Mao, and X. Yang (2016). Design Method for the Volute Profile of a Squirrel-Cage Fan with Space Limitation, *Journal of Turbomachinery* 138(8), 1-13.